Peer review status:

This manuscript is a non peer reviewed preprint submitted to EarthArXiv.

Title

Mid-crustal Origin of Alkaline Magmas in the Arosa Zone: Evidence from Primary Analcime and Xenolith Interaction at the Rothplattenbach Complex (Germany)

Authors & Affiliations

Alfred Wassermann[1] (a.wassermann@rmskempten.de)
Matthias Hanke[2] (hanke-matthias@t-online.de)

1. RMSKempten, Kempten. Germany
2. Independent researcher, Kempten. Germany

Corresponding Author

Alfred Wassermann (a.wassermann@rmskempten.de)

Journal Submission Status

Mid-crustal Origin of Alkaline Magmas in the Arosa Zone: Evidence from Primary Analcime and Xenolith Interaction at the Rothplattenbach Complex (Germany)

This is a non-peer-reviewed EarthArXiv preprint. May 2026

Authors: Dr. Alfred Wassermann (a.wassermann@rmskempten.de), Matthias Hanke (hanke-matthias@t-online.de)

Keywords: Primary analcime, closed-system differentiation, Rothplattenbach Complex, infiltration metasomatism, Jurassic limestone xenoliths, thermodynamic geobarometry, subduction channel, intrusive pillows, Arosa Zone, mid-crustal emplacement, European Cenozoic Rift System (ECRIS), water-saturated magmas, zeolite facies.

Abstract

The Rothplattenbach Complex (Arosa Zone, Germany) hosts alkaline magmatic rocks that provide unique insights into the mid-crustal evolution of water-saturated melts. This study presents a detailed phase-analytical investigation using XRD and SEM/EDX to characterize the primary magmatic mineralogy and its subsequent autometasomatic alteration. A key discovery is the occurrence of primary magmatic analcime, which, in equilibrium with anorthite-rich plagioclase (An77) and diopsidic clinopyroxene, serves as a precise geobarometer. Thermodynamic constraints require pressures of 5–6 kbar and temperatures below 660 °C for the crystallization of primary analcime, indicating that the magma solidified at mid-crustal depths of 15–20 km.

The petrogenetic evolution occurred within a closed system, where internally derived magmatic fluids triggered pervasive deuteric alteration. Depending on the local CO_2 fugacity, the system followed two distinct pathways: a zeolitic pathway ($X_{CO_2} < 0.02$) leading to the formation of thomsonite and natrolite, and a carbonate pathway ($X_{CO_2} > 0.02$) resulting in a calcite–natrolite–montmorillonite assemblage. The latter was locally triggered by the interaction with entrained Upper Jurassic red limestone xenoliths.

The coexistence of high-pressure magmatic phases and sedimentary xenoliths suggests a geodynamic setting within a subduction channel or tectonic mélange. In this environment, water-rich, unlithified sediments were transported to mid-crustal levels, where they encountered rising alkaline magmas. The resulting "intrusive pillows" and metasomatic reaction zones (including the formation of celadonite and monomineralic platy analcime) demonstrate that the characteristic pillow morphology was formed by expansion into a ductile, hydrous medium under high lithostatic pressure rather than by shallow-marine extrusion. These findings challenge traditional interpretations of the Arosa Zone magmatites and highlight the significance of primary analcime as a marker for deep-seated, water-saturated magmatism.

Introduction:
Already Carl Wilhelm von Gümbel. in his *Geology of Bavaria* (1888), documented the prominent outcrops of so-called “Alpenmelaphyre” at the Rothplattenbach. Blocks of these rocks are transported downstream to the Ostrach valley. These rocks, traditionally referred to as “spilites” of the Arosa Zone, crop out along a trail branching westward from the service road to the Hirschalpe (at ~1300 m a.s.l.). Field observations reveal dark basaltic debris locally replacing light carbonate lithologies along the path, and spilites are exposed in road cuts and float blocks along the ridge between the two streams.

Zeolites infilling vesicles and fractures in the Rothplattenbach spilites have been repeatedly reported. Additional occurrences of these spilites have been described from the Wildbach valley near Hindelang, the Retterschwang valley at the foot of the Rotspitze, Birgsau. the Geißalpe below the Entschenkopf, and the Ränkertobel at the Riedberg Pass. The rounded bodies, commonly interpreted as pillow lavas, are associated with marbleized carbonate rocks. Jurassic carbonate units. including Aptychus-bearing limestones, occur as associated lithologies. According to Scholz, the carbonate components represent tectonically sheared strata (red Aptychus limestone). Zeolites in these rocks have so far been interpreted exclusively as secondary alteration products of the magmatic body. However, this interpretation fails to explain the pervasive occurrence of analcime, particularly within the groundmass of the spilites.

Experimental constraints on the pressure–temperature dependence of analcime formation were already provided by Peters et al. (1966). Pearce (1970) investigated the Crowsnest Formation (Canada), which is well known for inferred primary analcime. Kim and Burley (1971) examined analcime stability fields at pressures up to 5000 bar, demonstrating for the first time that primary analcime may occur as a phenocryst phase in volcanic rocks. Luhr and Kyser (1989) discussed criteria for primary analcime in Mexican lavas, and Karlsson and Clayton (1991) provided one of the key frameworks for distinguishing primary from secondary analcime in igneous rocks. More recent studies, including the Mecsek Mountains study (2025), document analcime crystals in carbonate ocelli, interpreted as transitional between primary magmatic and hydrothermal origin.
In the investigated spilites, analcime occurs together with clinopyroxene and plagioclase as a constituent of the groundmass. This observation strongly argues against late, low-temperature hydrothermal zeolite formation and instead supports a primary magmatic or late-magmatic origin of analcime. This hypothesis, combined with a field excursion to the Rothplattenbach area in 2025, motivated a detailed phase-analytical investigation of spilite samples from the study area.


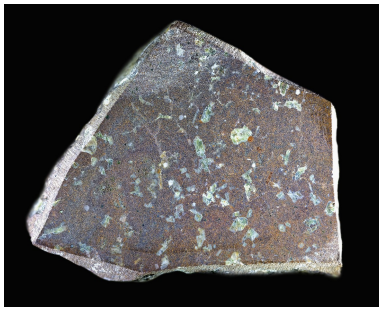
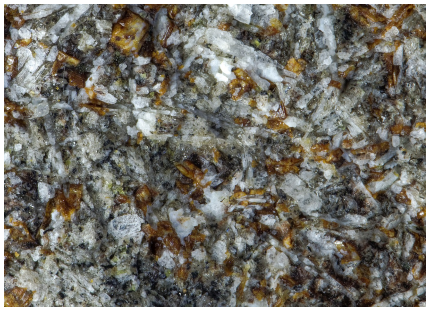

Figure 1: Groundmass of the magmatic rock. Plagioclase laths. clinopyroxenes. and analcime. Specimen: Width: 2.5 cm. Height: 1.5 cm. Depth: 0.6 cm. Image width: 3.2 cm. Mid: Split sample with polished surface. Width: ~ 5 cm. Right: Magnification showing the groundmass. Clearly visible are the large plagioclase molecules. the small brown analcims dispersed throughout the matrix. clinopyroxene microliths. and vulcanic glass in between. Photo: Matthias Hanke Collection

Primary analcime

Primary analcime has been reported mainly from silica-undersaturated alkaline magmatic rocks, such as basanites, phonotephrites, and certain lamprophyres. The question whether analcime is primary (crystallized from the melt) or secondary (formed by alteration of leucite) has been intensively debated in the literature. Chemical and mineralogical evidence supporting a primary origin has been presented in numerous studies.

Luhr and Kyser (1989) described analcime phenocrysts from the Colima volcanic complex (Mexico), where the groundmass consists of titanian salite (clinopyroxene), titanomagnetite, apatite, and abundant volcanic glass. The Crowsnest Formation in Alberta, Canada (blairmorites) is famous for centimetre-sized analcime crystals, widely interpreted as primary (Pearce 1993). These rocks are extremely alkaline and contain analcime (up to 30–50 vol%), sanidine, melanite garnet and aegirine–augite. Transitional varieties additionally contain plagioclase and diopside in the groundmass.

Analcime-bearing basanites from the Westerwald and the Hessian Depression commonly contain diopsidic augite and plagioclase (typically labradorite to bytownite, rarely pure anorthite) together with analcime in the groundmass. Tephritic analcimites from the České středohoří (Bohemian Massif) exhibit primary analcime in the groundmass associated with clinopyroxene and plagioclase laths. In the Colli Albani volcanic district (Italy), analcime-bearing rocks show parageneses with diopsidic clinopyroxene and very Ca-rich plagioclase (An contents > 80–90%). Analcime phonolites and tephritic rocks from the Kaiserstuhl volcanic complex also commonly contain primary analcime, particularly in transitional facies towards analcime-bearing basanites (limburgites). The Monzoni intrusive complex (Dolomites), although largely plutonic, displays a closely comparable mineral assemblage with fassaite (Ti-diopside), anorthite, and analcime.

In the Hegau volcanic field (e.g. Höwenegg. Stoffeln), analcime basanites and analcimites occur, and the groundmass typically contains diopsidic augite and plagioclase. Plagioclase laths commonly range from An_{70} to An_{85}. Extensive geochemical data demonstrate that these melts were extremely silica-undersaturated and water-rich, conditions favourable for primary analcime crystallization. Huckenholz (1977) provided major-element compositions (SiO_2. Al_2O_3. Na_2O. K_2O. etc.) indicating that analcime crystallized directly from the residual melt. Wilson and Downes (1991) presented geochemical data for Hegau alkaline basalts, including analcime-bearing varieties, in a European context.

In melilite–analcimites from the Urach–Kirchheim volcanic field (Swabian Alb), analcime commonly occurs as a primary groundmass phase. Although melilite is the dominant phase, less undersaturated varieties (“basalts”) also contain bytownitic plagioclase and diopside. Mäder (1983) reported detailed geochemical data for melilitites and analcimites, showing high Na_2O/K_2O ratios, which favour analcime over leucite formation. Analcime phonolites and tephritic dykes from the Kaiserstuhl also widely contain primary analcime, and plagioclase in mafic varieties reaches very

high anorthite contents (up to An_{90}). The association of Ca-rich plagioclase with primary analcime is a strong indicator of high water vapour pressure (P_{H2O}). High melt water contents stabilize anorthite relative to albite and simultaneously allow analcime to crystallize directly from the melt. This combination is characteristic of differentiated magmas in continental rift settings of southern Germany.

Experimental studies by Roux and Hamilton (1976) in the $NaAlSi_3O_8$–$NaAlSiO_4$–H_2O system demonstrated that primary analcime is stable only within a narrow temperature window (<650 °C at P_{H2O} = 5 kbar). Thus, the melt must remain liquid at these low temperatures, requiring an appropriate eutectic composition. Experimental stability curves by Huckenholz (1977) and Roux and Hamilton (1976) are critical for the present study, as they define the P–T conditions under which a melt of the composition observed in the Rothplattenbach magmatites can precipitate analcime.

Primary analcime exhibits a lower pressure limit and an upper temperature limit: below ~2.3 kbar analcime is unstable as a magmatic phase and decomposes to nepheline + albite + vapour. Even at high pressure, analcime melts incongruently at relatively low temperatures. At pressures above 5 kbar, the thermal stability limit is ~650–660 °C. Because basaltic melts (clinopyroxene + plagioclase) normally crystallize at temperatures >900 °C, primary analcime can only form if high water contents keep the residual melt liquid down to <650–660 °C.

The maximum stability temperature of analcime can be approximated by:

$$T = 600 + 15 \cdot (P - 2).$$

where T is in °C and P in kbar. At 5 kbar, this yields a maximum stability of ~645–655 °C, increasing to ~655–665 °C at 6 kbar. These constraints explain why primary analcime occurs in Hegau magmas under such conditions, whereas drier or more K-rich magmas (e.g. parts of the Kaiserstuhl) preferentially crystallize leucite or nepheline.

Magma evolution in a closed system

Sample 4 represents a rock body previously described as “spilite” and lacking xenoliths of Jurassic red limestone. From this sample, three subsamples (a–c) of the dark-brown magmatic groundmass were collected and analysed by X-ray diffraction phase analysis.

Figure 2: Sample 4: Left: Split sample with polished surface. Width: ~ 5 cm. Right: Magnification showing the groundmass (width 1 mm). Brown analcime crystals with sharp. clear edges. black clinopyroxene microliths and bluish plagioclase laths. Photo: Matthias Hanke Collection

All three analyses identified the zeolite analcime; thomsonite was additionally detected in samples (b) and sample (c). Anorthite-rich plagioclase was present in all samples. Calcite detected in the samples (a) and (b) was introduced during sample preparation from calcite veins and is therefore not considered a primary magmatic phase (Figure 3).

We interpret the system as closed, with no material influx into or outflux from the groundmass.

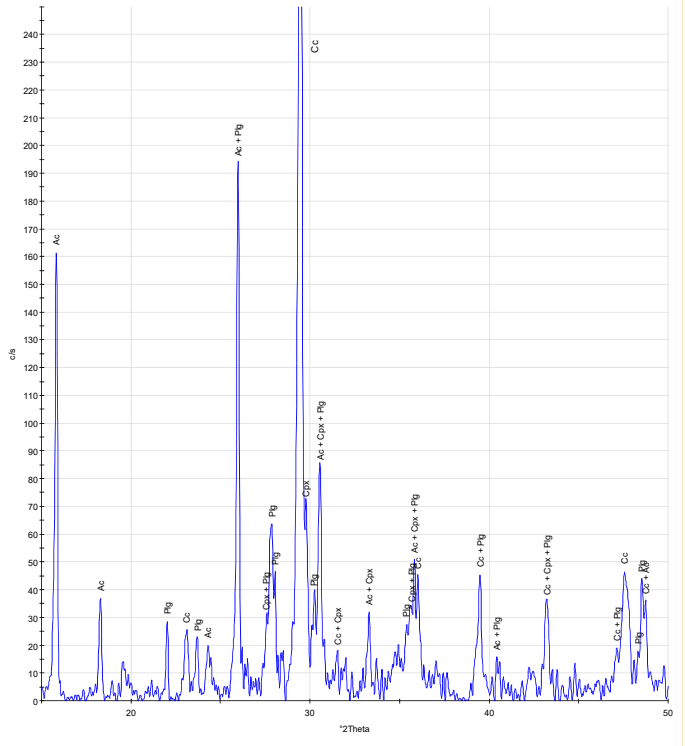

Figure 3: X-ray diffractogram of the matrix of sample 4a. Interferences of analcime (Ac). plagioclase (Plg77). and diopsidic clinopyroxene (Cpx) are clearly visible. The detected calcite (Cc) originates from sample preparation rather than the primary matrix.

The groundmass of the investigated magmatic rock consists of plagioclase, clinopyroxene, analcime, thomsonite and an amorphous component. The mean phase concentrations derived from the XRD analyses of the sample 4 groundmass are:

Analcime (wt%)	Thomsonite (wt%)	Clinopyroxene (wt%)	Plagioclase (wt%)
20.10 ± 0.87	7.63 ± 0.79	14.34 ± 1.52	57.93 ± 3.28

Initial magma composition

Based on the analytical data, the initial composition of the magma can be defined with high confidence. The normative bulk rock composition was calculated from multiple quantitative XRD phase analyses of the groundmass, H_2O represents the stoichiometric water content of the identified zeolite phases. It corresponds to the blue-shaded field in the compositional triangle (see Figure 4) at 650°C < T < 1100 °C and P > 5 kbar, consistent with a basaltic magma composition.

Oxides	wt%	±
SiO_2	48.58	2.01
Al_2O_3	24.37	0.84
Fe_2O_3	2.86	0.11
MgO	3.03	0.12
CaO	13.5	0.32
Na_2O	4.24	0.24
K_2O	0.49	0.07
H_2O_{calc}	2.86	0.15
Sum	100	

The composition of the plagioclase solid solution was determined from lattice parameters, in particular the unit-cell volume V_0.

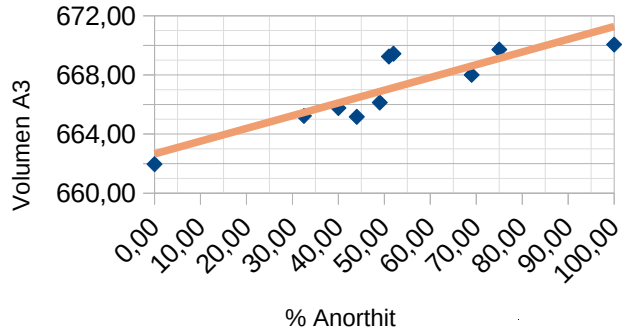

Figure 4: Cell volume V_0 range between albite and anorthite based on values from the ICDD PDF-5 database. The orange line represents the linear regression: (An % = (V_0 – 662.65372) / 0.086161).

The mean unit-cell volume of the measurements is 669.308 Å³. corresponding to an anorthite content of ~77 (± 5) wt%. The calculated composition of the plagioclase is $Ca_{0.77}Na_{0.23}Al_{1.77}Si_{2.23}O_8$.

The term “spilite” traditionally refers to hydrothermally altered (albitized) basalts. We use the term here only in a historical sense, as the measured plagioclase composition (An_{77}) clearly excludes a spilite sensu stricto (which would require An < 10).

The composition of clinopyroxene (Cpx) was also derived from lattice-parameter analyses.

Parameter	Å/degree	±
a_0	9.725	0.059
b_0	8.878	0.075
c_0	5.272	0.030
beta	106.162	0.887

Clinopyroxene lattice parameters. Average values across all nine samples.

According to the ICDD PDF-5 Database, the detected clinopyroxene is a Na-, Fe-, and Al-bearing diopside with the composition $Ca_{0.955}Na_{0.045}Mg_{0.89}Fe_{0.133}Si_2O_6$.

The mean lattice parameter a_0 of the detected analcime is 13.724 ± 0.011 Å. This value is in very good agreement with the analcime values from the ICDD PDF5 database of 13.719 ± 0.010 Å for the chemical formula $NaAl(Si_2O_6) \cdot H_2O$ with the Si/Al ratio of 2.

Pressure–temperature constraints

The mineral assemblage provides independent constraints on pressure and temperature. The occurrence of primary analcime requires pressures > 5 kbar. In hydrous systems, the diopside solidus at 5 kbar is ~1100 °C, marking the onset of crystallization (Yoder, Roy, and Tuttle 1956). A plagioclase composition of An_{77} implies pressures > 6 kbar at 800 °C (Yoder et al.. 1956).

To illustrate the chemistry of the relevant phases, the quaternary system nepheline–K-feldspar–anorthite–quartz is commonly used (after Yoder or Schairer). For a better visualization of zeolite phases, we instead use the subtriangle $Na_2Al_2Si_2O_8$–Anorthite ($CaAl_2Si_2O_8$)–Quartz (SiO_2), where $Na_2Al_2Si_2O_8$ represents the carnegieite/nepheline component. This triangle covers the entire compositional range from basaltic melts to strongly silica-undersaturated compositions. Analcime plots within this triangle (as a mixture of the Na component and quartz/H_2O), allowing graphical representation of melt evolution across the field.

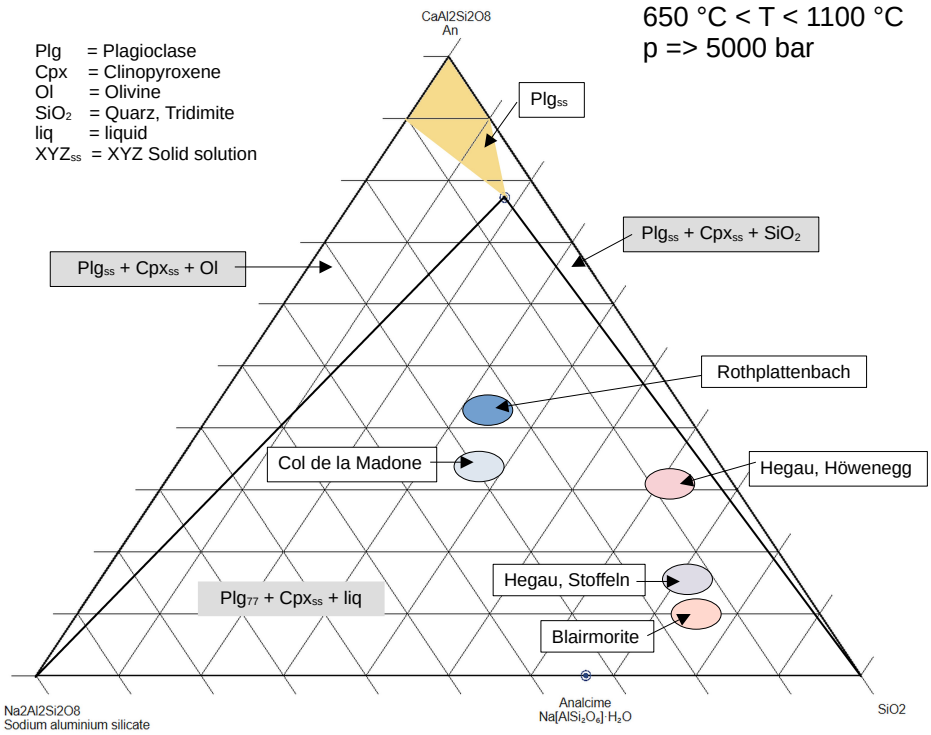

Figure 5: Compositional triangle at T > 650 °C.

Phase relations and fractional crystallization

At temperatures of 900–1100 °C and pressures > 5 kbar, the diagram sidplays the plagioclase solid-solution field and three phase fields. In the Na/Ca-rich domain, the assemblage Cpx_{ss} + Plg_{ss} + olivine is stable, whereas in the Ca/Si-rich domain the assemblage Cpx_{ss} + Plg_{ss} + SiO_2 occurs. Between these fields lies the extensive Cpx_{ss} + Plg_{ss} + liquid field; only this central field contains melt, whereas the two outer fields are fully crystalline.

Starting at ~1100 °C, decreasing temperature drives continuous cotectic crystallization. Components crystallize steadily from the melt, the melt fraction decreases, its composition evolves, and the Cpx/Plg_{ss} ratio adjusts accordingly. This melt evolution can be modelled using Rayleigh fractional crystallization. To evolve from an average basaltic starting composition (Rothplattenbach)

to the composition of analcime in a closed system, approximately 72–75% of the initial material must crystallize as clinopyroxene + plagioclase. This process results in residual enrichment of incompatible components (Na_2O and H_2O), such that the final residual melt (~25%) crystallizes as analcime.

The late-magmatic evolution towards analcime can thus be fully reconstructed within a phase-equilibrium framework. Between ~800 °C (P > 6 kbar; plagioclase formation) and the analcime stability limit (<660 °C), a cooling window of ~150 K exists. Within this interval, removal of Cpx and An_{77} must drive the melt composition to converge precisely on the analcime composition at ~660 °C. Since the pressure (> 6 kbar) is well above the critical analcime threshold (~2.3 kbar), the only remaining variable controlling analcime saturation is the attainment of sufficient H_2O activity in the residual melt.

The compositional triangle includes not only the starting composition of the Rothplattenbach magma (blue field) but also initial magma compositions from Hegau–Höwenegg, Hegau–Stoffeln, blairmorites and Col de la Madone. All plot within the same three-phase field. This indicates that primary analcime formation is not a local peculiarity of Rothplattenbach, Kaiserstuhl or Hegau, but follows strict thermodynamic constraints. If a magma starts within the Cpx_{ss} + Plg_{ss} + liquid field, cotectic crystallization of clinopyroxene and plagioclase forces residual melts into the same compositional „bottleneck“, leading to chemical convergence toward the analcime composition. The fact that diverse initial compositions—from intermediate blairmorites to mafic Hegau basanites—plot in the same field and all contain primary analcime strongly supports this hypothesis.

Post-magmatic (autometasomatic) evolution in a closed system

With crystallization of primary analcime, the residual melt is exhausted. The rock is now fully solidified but remains mineralogically highly reactive.

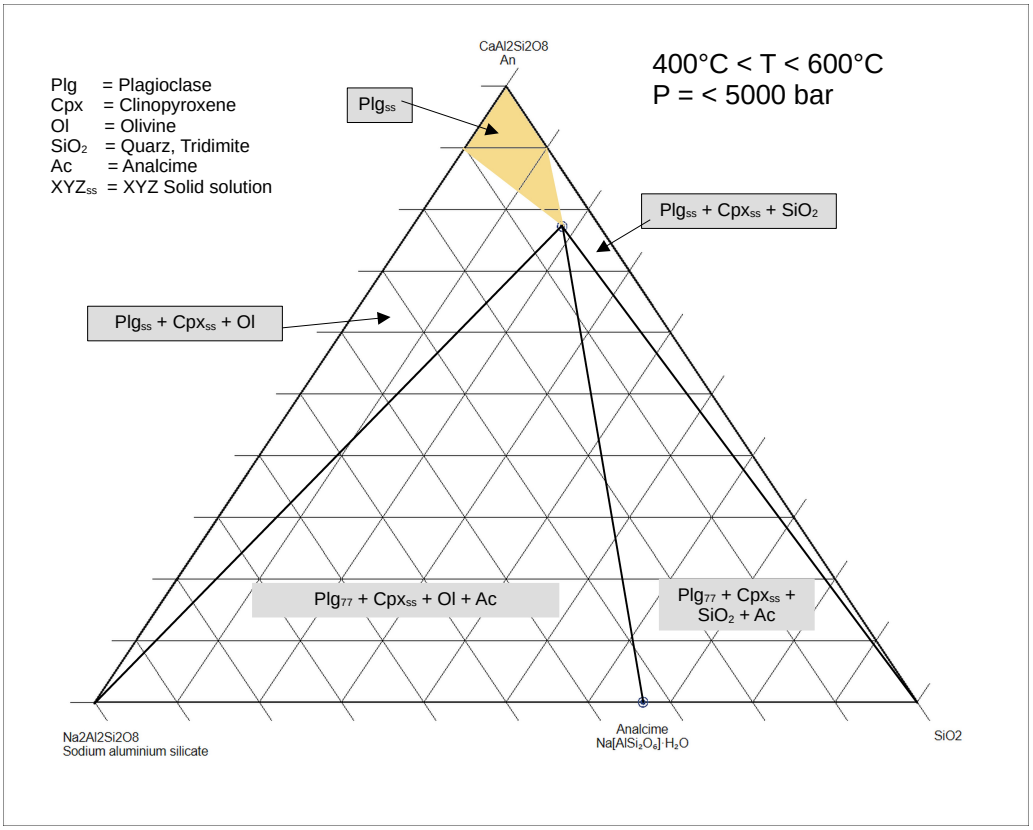

Figure 6: Compositional triangle at 400–600 °C.

Upon complete solidification, an fluid phase is released and these hot fluids circulate along grain boundaries. During further ascent to shallower crustal levels, pressure decreases below the critical threshold of 5 kbar. The preservation of primary analcime in our samples requires either sufficiently rapid cooling to prevent decomposition into nepheline + albite + H_2O, or persistently high H_2O contents that expand the analcime stability field toward lower pressures. Analcime is characterized by an open zeolitic framework, enabling extensive Na^+ exchange with other cations and further hydration processes. The now-stable plagioclase (An_{77})–analcime conode defines the boundary between basaltic (olivine-bearing) and andesitic (quartz/tridymite-bearing) magma compositions.

The mineral assemblages illustrated in the compositional triangle remain stable at temperatures below 600 °C and a pressure of 5 kbar. Upon further slow cooling, the system releases fluids at approximately 400 °C, with the exact temperature being a function of the CO_2 fugacity within the fluid phase.

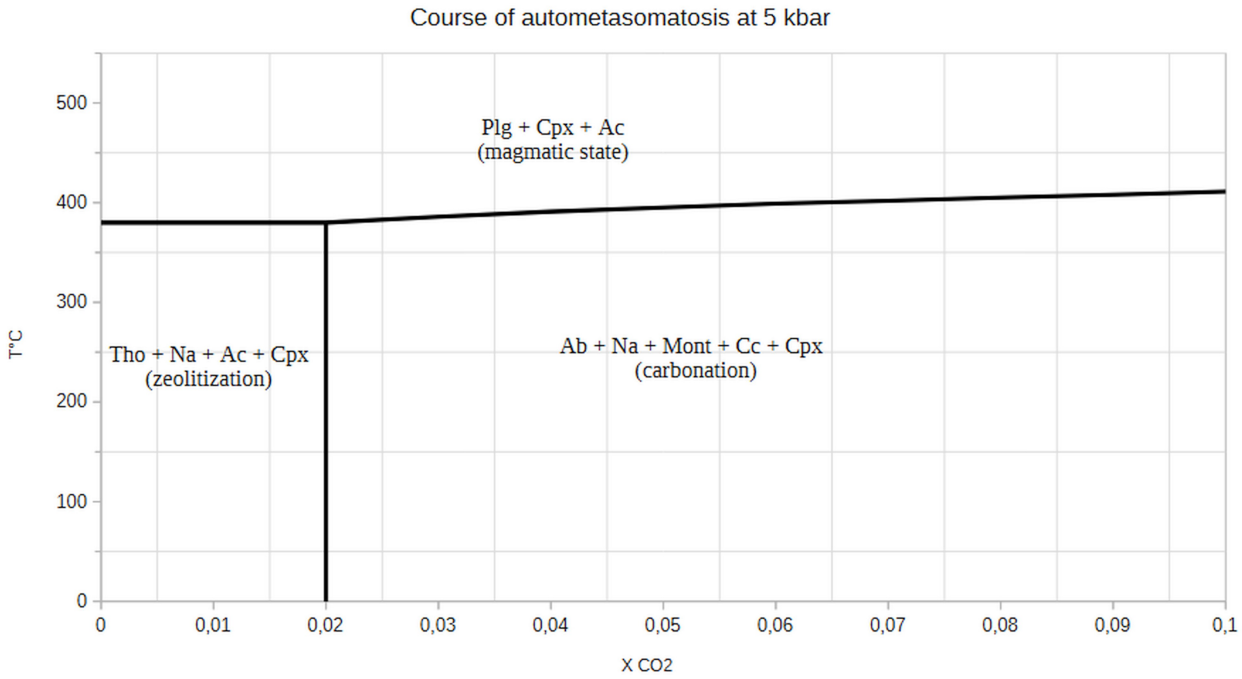

Fig. 7 Calculated equilibrium curves of the discussed autometasomatic reactions. The calculation of the equilibrium curves is based on minimizing the Gibbs free energy (ΔGrxn = 0) of the reactions for:
a) Zeoliteization: $NaAlSi_3O_8$ (Ab component) + 2 $CaAl_2Si_2O_8$ (An component) + 6 H_2O ⇌ $NaCa_2Al_5Si_5O_{20}$· 6H_2O + 2 SiO_2
b) Carbonation: 1 $CaAl_2Si_2O_8$ + 2.30 $NaAlSi_2O_6$·H_2O + 0.86 H_2O + 0.86 CO_2 ⇌ 1.15 $Na_2Al_2Si_3O_{10}$·2H_2O + 0.86 $Ca_{0.165}Al_{2.33}Si_{3.67}O_{10}(OH)_2$ + 0.86 $CaCO_3$

The temperature threshold of approximately 400 °C marks the transition from the magmatic high-temperature stage to the autometasomatic low-temperature stage. The phase boundary at X_{CO_2} = 0.02 separates the stability fields of zeolitization and carbonation.

Phase Relations and Zeolitic Reactions

At $X_{CO_2} < 0.02$ (zeolitization), thomsonite forms from plagioclase on the Na-rich side of the composition triangle:

$NaAlSi_3O_8$ (Ab component) + 2 $CaAl_2Si_2O_8$ (An component) + 6 H_2O ⇌ $NaCa_2Al_5Si_5O_{20}$· 6H_2O + 2 SiO_2

In a closed system, the hydration of plagioclase to zeolites results in significant volume expansion. This process induces microfracturing, which facilitates fluid circulation and the subsequent formation of late-stage mineral phases.

On the SiO_2-rich side of the triangle, the liberated SiO_2 reacts with the anorthite component of plagioclase just below 400 °C to form wairakite:

Plgss + SiO_2 + H_2O ⇌ Wairakite
$CaAl_2Si_2O_8$ (An component) + 2 SiO_2 + 2 H_2O ⇌ $CaAl_2Si_4O_{12}$·2H_2O

Simultaneously, the albite component of the plagioclase solid solution (Plg_{ss}) reacts to form natrolite at the base of the composition triangle:

Plgss ⇌ Natrolite + SiO_2

2 $NaAlSi_3O_8$ ⇌ $Na_2Al_2Si_3O_{10}·2H_2O$ + 3 SiO_2

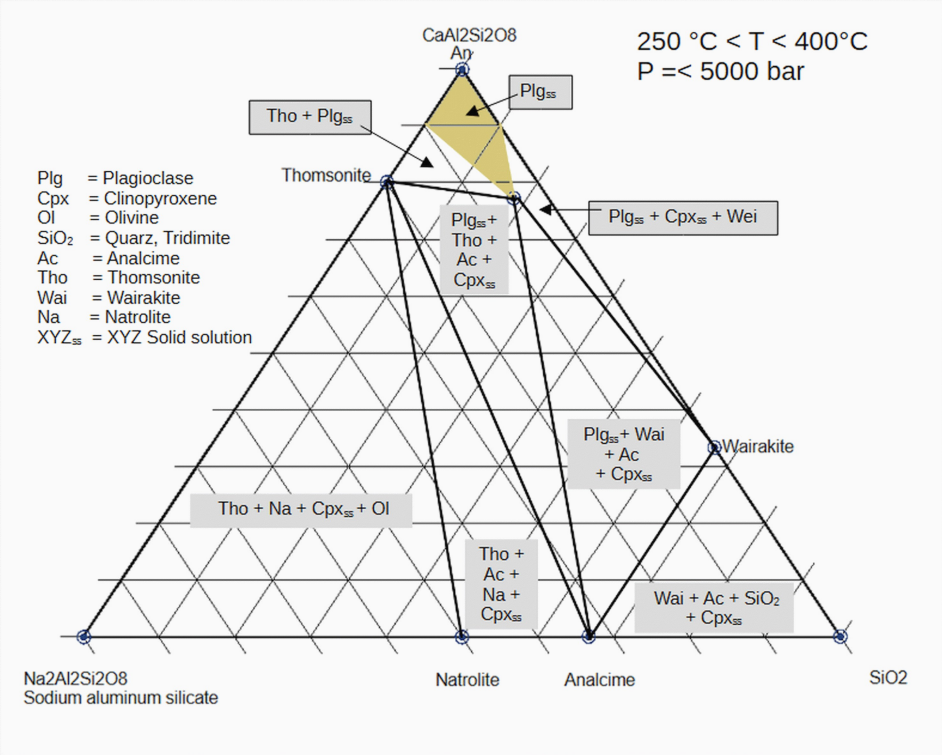

Figure 8: Compositional triangle at 250–400 °C.

As cooling progresses below 250 °C. wairakite hydrates to laumontite:

$Ca[Al_2Si_4O_{12}]·2H_2O$ (wairakite) + 2 H_2O ⇌ $Ca[Al_2Si_4O_{12}]·4H_2O$ (laumontite).

The SiO_2 released during natrolite formation reacts with the anorthite component of plagioclase and H2O to produce heulandite:

4 $CaAl_2Si_2O_8$ + 20 SiO_2 + 24 H_2O ⇌ $Ca_4Al_8Si_{28}O_{72}·24H_2O$

Below 150 °C. laumontite further hydrates to chabazite:

$Ca[Al_2Si_4O_{12}]·4H_2O$ (laumontite) + 2 H_2O ⇌ $Ca[Al_2Si_4O_{12}]·6H_2O$ (chabazite).

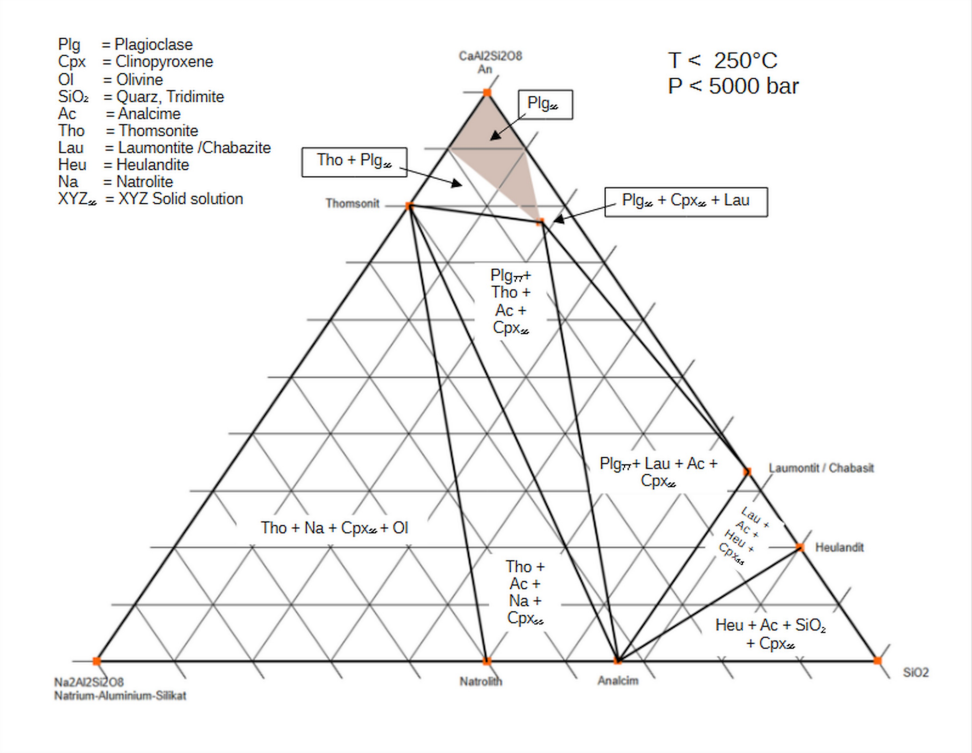

Figure 9: Compositional triangle at T < 250 °C.

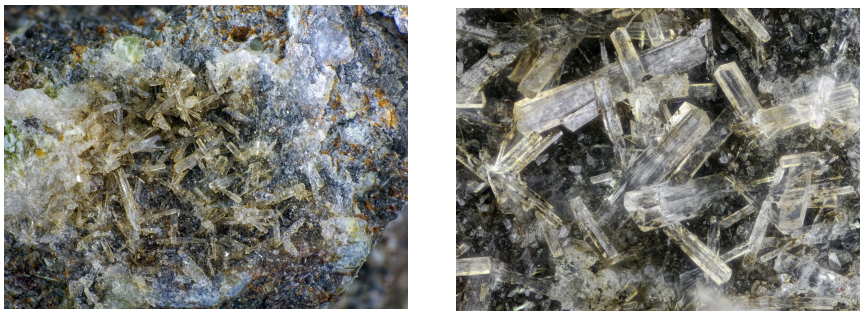

Figure 10: Magnifications of Ac + Na + Tho + Cpx_{ss} parageneses (width 4mm). Left: Visible are the zeolites Ac (red in the background, Tho (light brown), Na (white). Right: Tho + Na (width 1,2 mm).

Phase Relations and Carbonation Reactions

If the X_{CO_2} of the fluid phase exceeds 0.02. the anorthite component of plagioclase reacts with analcime, H_2O and CO_2 to form a secondary mineral assemblage of natrolite, montmorillonite and calcite according to the following reaction:

$$1\ CaAl_2Si_2O_8 + 2.30\ NaAlSi_2O_6{\cdot}H_2O + 0.86\ H_2O + 0.86\ CO_2 \rightleftharpoons$$
$$1.15\ Na_2Al_2Si_3O_{10}{\cdot}2H_2O + 0.86\ Ca_{0.165}Al_{2.33}Si_{3.67}O_{10}(OH)_2 + 0.86\ CaCO_3$$

The introduction of CO_2 from the fluid phase expands the previous ternary compositional triangle into a quaternary tetrahedron. Calcium, formerly hosted in the anorthite component of plagioclase, is partitioned into the newly formed calcite phase. Consequently, the former analcime–plagioclase (An_{77}) tie-line is replaced by the three-phase stability field natrolite–montmorillonite–calcite. The albite component (approximately 0.3 mol per mol of the original carbonated An_{77}) does not

participate in this specific reaction and remains as residual albite within the paragenesis. This phase relationship is illustrated in the subsequent compositional diagram.

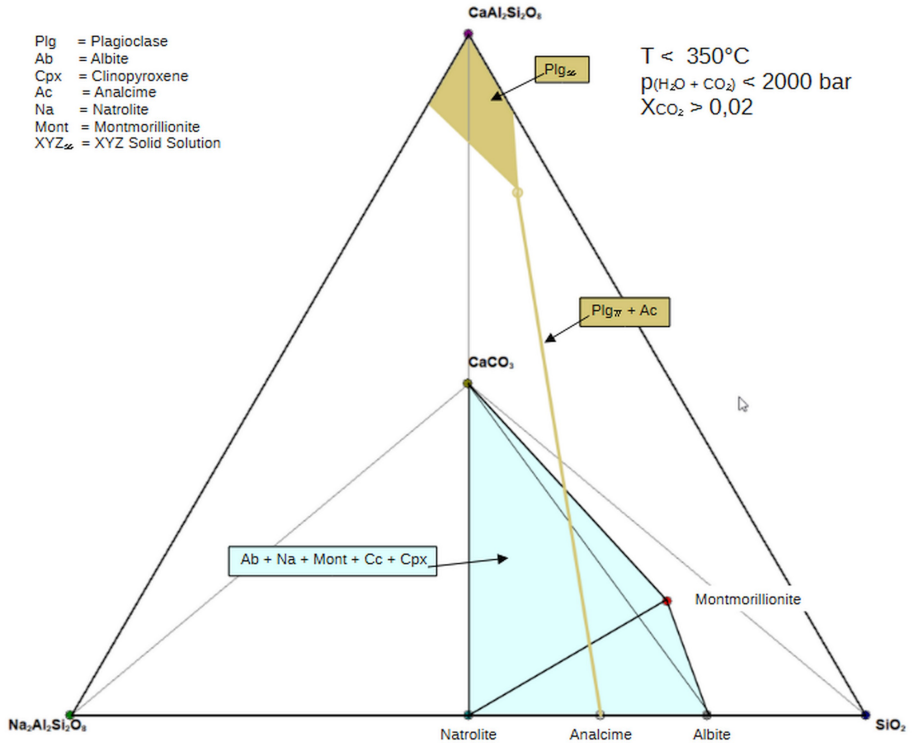

Figure 11: Compositional triangle at T < 350 °C.

Figure 12: Petrographic analysis of sample 4. Left: Polished section (approx. 5 cm width). Middle: Detailed micrograph of the reaction textures. The dark matrix hosts large plagioclase phenocrysts. finely dispersed brown analcime, and acicular clinopyroxene. The prominent white, rounded domains are products of the autometasomatic, post-magmatic evolution in a closed system. These domains predominantly consist of calcite, montmorillonite, and natrolite. The reaction front is clearly discernible. Within this zone. analcime has been almost entirely consumed, reacting with plagioclase to form the secondary assemblage. Plagioclase crystals outside this reaction zone remain pristine and unaffected by the carbonation process. *Photos: Matthias Hanke Collection.*
Right: SEM image of a carbonated plagioklas.

SEM/EDX Methodology and Data Interpretation

Due to the absence of a conductive coating (carbon or gold), the EDX analyses were affected by significant surface charging. This led to localized deflection of the primary electron beam and "remote excitation" effects. Consequently, the acquired data predominantly represent mixed signals from fine-grained mineral aggregates rather than single-phase analyses. To resolve these phases, a normative deconvolution was performed using atomic ratio plots.

1. Si/Al Ratio Plot (Phase Identification)
Stoichiometric Si/Al ratios serve as a robust indicator for identifying the reacting phases. Anorthite has an Si/Al ratio of 1.0, natrolite of 1.5, analcime and montmorillonite of ~2.0 an pure albit of 3.0.

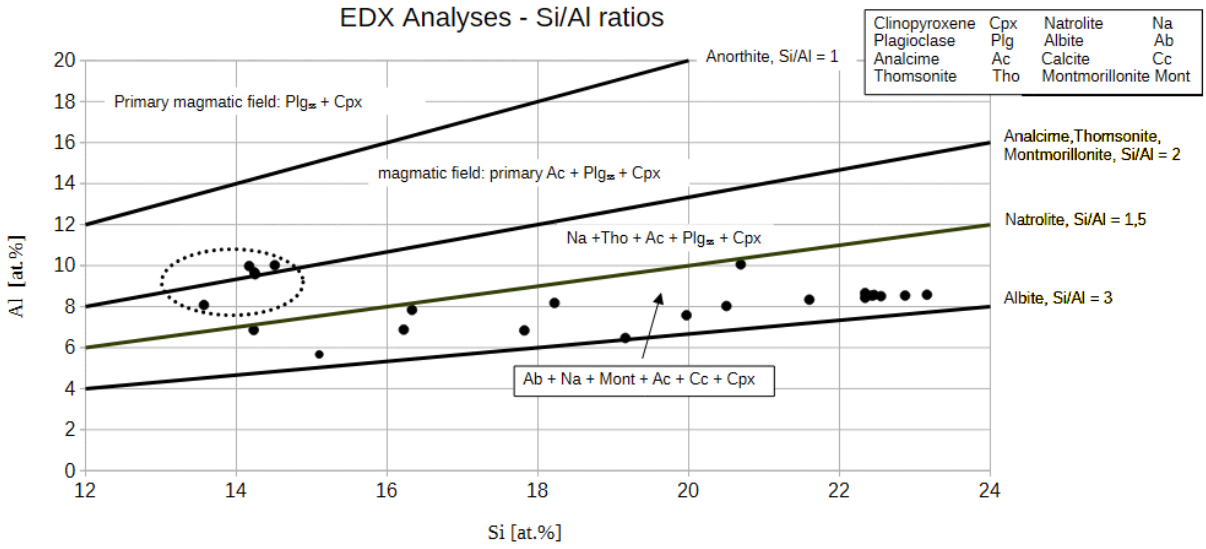

Figure 13: Plot of atomic % Al vs. atomic % Si: The axes are scaled to highlight compositional trends between magmatic precursors and alteration products. Data points represent mixed signals due to beam-charging effects on uncoated samples. The distribution defines a reaction pathway originating from the anorthite-rich plagioclase (Plg_{ss}) and analcime (Ac) fields (circled) toward the more Si-rich domains of natrolite and montmorillonite. The clustering between endmembers indicates incomplete reaction progress, characteristic of rapid cooling in a closed system.

The scatter plot of the EDX data reveals that the majority of measurements cluster between these endmembers, documenting the breakdown of the magmatic primary assemblage. The presence of data points near the Plg_{ss} and analcime fields indicates that the reaction was kinetically limited and did not reach completion during the rapid cooling of the system.

2. O/Ca Ratio Plot (Evidence for Carbonation)
To quantify the extent of carbonation, the O/Ca ratio was utilized. Pure calcite is characterized by an ratio of 3.0, whereas montmorillonite exhibits a significantly higher ratio of approximately 20 (depending on hydration state). Additionally, stoichiometric lines fot thomsonite (O/Ca = 5.0) and anorthite (O/Ca = 8.0) were plotted.
The measured data points show an accumulation in the region where zeolitic and carbonate alteration occur during cooling in a closed system. Another accumulation is found near the Ca [at%] = 0 axis; these points exhibit an O/Ca ratio corresponding to that of pure analcime. The data form a linear trend between these values, providing compelling evidence for the presence of sub-

microscopic calcite within the plagioclase alteration zones. The results demonstrate two distinct states: the late magmatic and the autometasomatic state. They reflect the zeolitic (thomsonite + analcime + plagioclase) and carbonate (albite + montmorillonite + calcite) transformation of anortite-rich plagioclase in a closed system, depending on the CO_2 content of the fluid phase. This confirms that the observed "mixed signals" result either from the intimate intergrowth of calcite and smectites during carbonation or thomsonite and plagioclase during zeolitization.

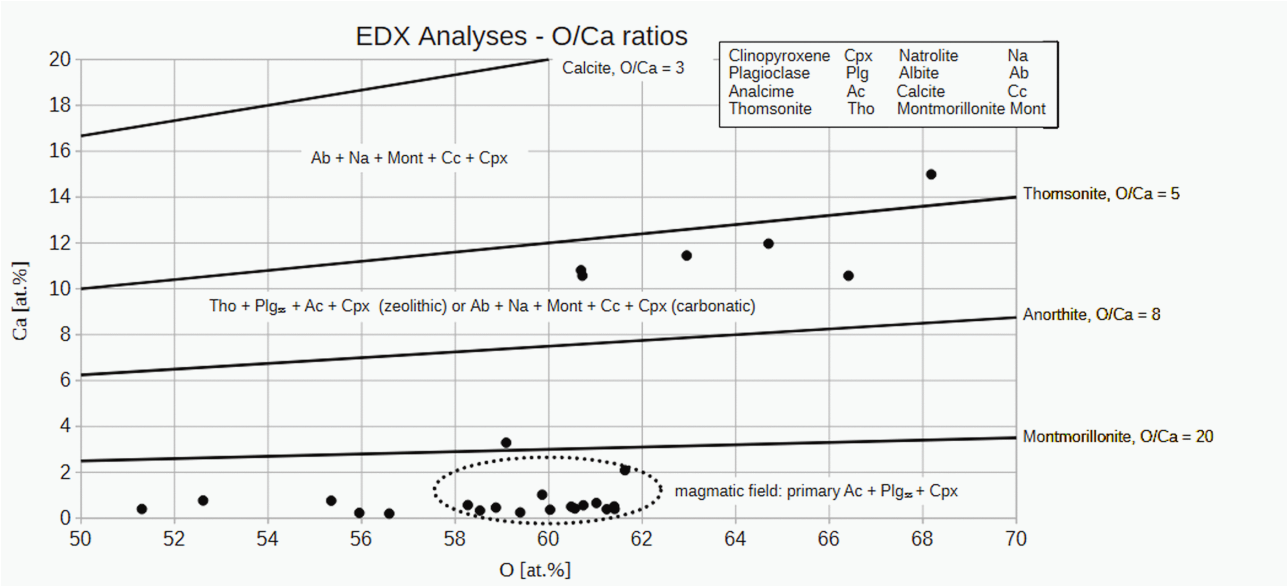

Figure 14: Plot of atomic % Ca vs. atomic % O: This diagram illustrates the carbonation of the primary plagioclase. The measured points define a linear mixing trend between the montmorillonite pole (high O/Ca ratio) and the calcite pole (O/Ca=3). This trend provides quantitative evidence that the secondary mineralogy consists of a sub-microscopic intergrowth of smectites and calcite, triggered by CO_2-bearing magmatic fluids. Points circled near the Ca = 0 line represent analcime with no or negligible calcium content. Their spatial separation from the carbonated zones support the hypothesis that analcime crystallized as a primary phase before Ca-rich fluids from the xenolith interaction or plagioclase degradation became active. The data cluster along a reaction pathway from the Plg_{ss}-analcime field toward thomsonite and montmorillonite, indicating autometasomatic processes in a closed system. Local shifts toward the calcite line reflect interaction with carbonate xenoliths.

Interaction with xenoliths

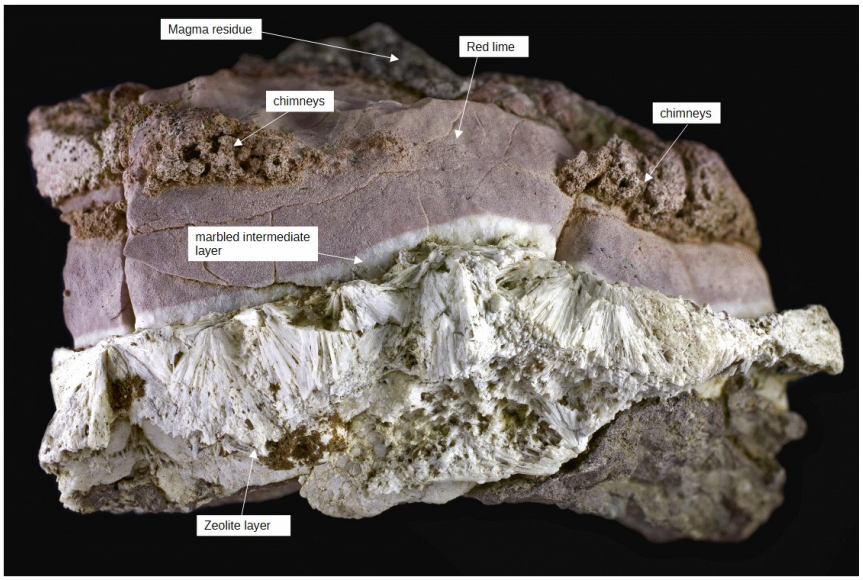

Figure 15: Sample 1

Dimensions:
Width (cm): 9
Height (cm): 6
Depth (cm): 4

Photo:
Matthias Hanke Collection

Figure 15 shows a sample from the Rothplattenbach area illustrating thermometamorphic reactions at the contact between red Jurassic limestone and the magma. These red limestones have previously been interpreted as entrained sedimentary blocks. XRD phase analysis of the limestone in this sample indicates a monomineralic calcite assemblage. The lattice parameters of the limestone calcite are:

The lattice parameters of the limestone calcite are:
a_0 = 4.989 ± 0.001 Å. c_0 = 17.057 ± 0.015 Å, V_0 = 367.61 ± 1.6 Å³, c/a = 3.419

Moving downward in the image, the red limestone transitions into a relatively thin white intermediate layer, followed by a thick zeolite layer. The white intermediate layer also consists of pure calcite. Its diffractogram shows significantly higher counting statistics compared to the limestone, while the crystallinity (1361 counts/2θ) is much lower than that of the limestone (38,659 counts/2θ). The lattice parameters of this intermediate-layer calcite are:
a_0 = 4.989 ± 0.007 Å, c_0 = 17.12 ± 0.07 Å, V_0 = 369.18 ± 3.9 Å³, c/a = 3.431

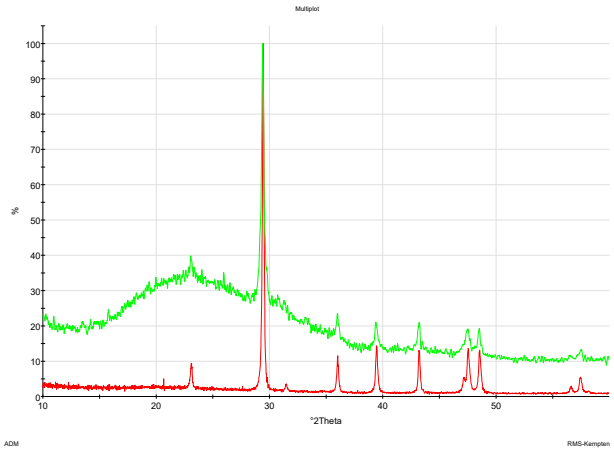

Figure 16: X-ray difractograms of the red limestone (red) and the marbled. white intermediate layer (green). The high proportion of amorphous material in the marbled intermediate layer is clearly visible.

The contact between the Jurassic limestone and the magma did not produce classical skarn mineralization, but rather a narrow zone of isochemical recrystallization. The expansion of the calcite lattice in the intermediate layer (c_0 from 17.057 Å to 17.12 Å), accompanied by a collapse in crystallinity, documents a rapid thermal pulse. During recrystallization, red-staining impurities were segregated, and pure white calcite crystallized.

The absence of wollastonite supports the inference of high lithostatic pressure (> 5 kbar) during magma evolution, suppressing calcite decarbonation. The overlying zeolite-rich layer marks the boundary where fluids from the H_2O-saturated magma interacted with recrystallized marble.

At the contact zone, the hot magma encountered the cooler limestone xenolith. This triggered a vigorous mobilization of elements between the calcium-rich xenolith and the sodium-dominated magma. At high contact temperatures (> 800 °C), part of the limestone became marbled; this chemical barrier subsequently limited the exchange of substances between the xenolith and the magma. As temperatures continued to fall, the zeolite layer formed within the system, which remained effectively closed due to this chemical barrier. The formation of the zeolite layer originated from the extensive exsolution of water from the magma at the contact as temperature decreased. The sharply diffracting natrolite indicates undisturbed crystal growth in a stable hydrothermal halo and confirms our assumption that primary analcime formation occurred in a water-saturated melt at pressures > 5 kbar.

Fluid-escape structures and magmatic residues

Above the limestone in sample 1. chimney-like. upward-open structures embedded in magmatic material occur. These structures were initially interpreted as CO_2 fluid-escape conduits formed during thermal decomposition of calcite. However, phase analysis shows that these structures consist solely of analcime–natrolite aggregates. The absence of CaO or Ca-silicate phases refutes thermal decomposition of the limestone. Instead, these structures record the directed ascent of magmatic fluids injected into the surrounding magmatic matrix, a consequence of the low permeability of the limestone xenolith. This confirms an H_2O-saturated system under high lithostatic pressure, where the stability limit of calcite was not exceeded.

Phase analysis of magmatic residues in sample 1 shows plagioclase, clinopyroxene, and zeolites (thomsonite and analcime). The calcite detected is likely preparation-related contamination from the underlying limestone. Notably, quartz is absent. The coexistence of primary clinopyroxene and plagioclase with analcime and thomsonite demonstrates that cooling and hydration followed the same closed-system petrogenetic pathway, even in direct proximity to the xenolith. Local natrolite enrichment in chimney structures reflects the mechanical segregation of fluid-rich residual phases, whereas the main magma preserved its mineralogical identity (Plg_{77}–analcime cotectic) up to the contact.

Progressive xenolith interaction (samples 2 and 3)

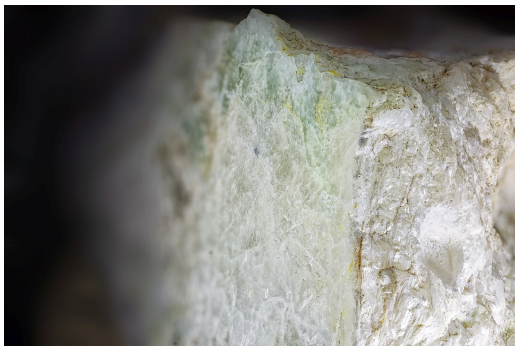

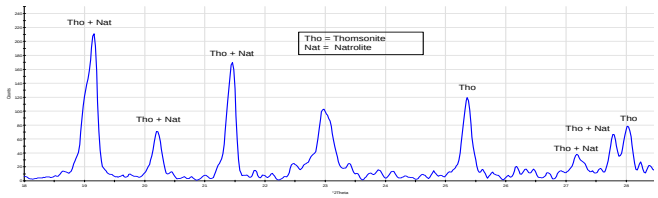

Figure 17: Sample 2: Dimensions: Width (cm): 14. Height (cm): 6.5. Depth (cm): 4. The sampling point on this sample can be seen in the right part of the image. Photo: Matthias Hanke Collection. The XRD diffractogramm showing the main interferences of thomsonite and natrolite.

Sample 2 contains a polished white domain analyzed by XRD. The diffractogram background between 15° and 40° 2θ indicates an amorphous component > 20 wt%. In addition to calcite, thomsonite and natrolite were identified. In contrast to the purely physical marbling observed in sample 1, sample 2 documents intense chemical interaction. The amorphous fraction suggests local melting (palingenesis) or the formation of a viscous silicate glass phase produced by the reaction of magmatic fluids with the xenolith. The coexistence of thomsonite and natrolite indicates hybridization between magmatic Na and carbonate-derived Ca. The amorphous "hump" is consistent with a polymerized silicate structure typical of quenched, H_2O-rich-rich residual melts or zeolitic precursors.

Figure 18: Sample 3

Dimensions:
Width (cm): 11
Height (cm): 12
Depth (cm): 8

Photo: Matthias Hanke Collection

Sample 3 contains a limestone xenolith crosscut by white veins. Three subsamples were analyzed. Phase analysis indicates > 57 wt% amorphous material; crystalline phases include analcime (13 wt%), thomsonite (35 wt%), natrolite (25 wt%), wairakite (9 wt%), clinopyroxene (8 wt%), calcite (3 wt%), celadonite (5 wt%), and vermiculite (4 wt%).

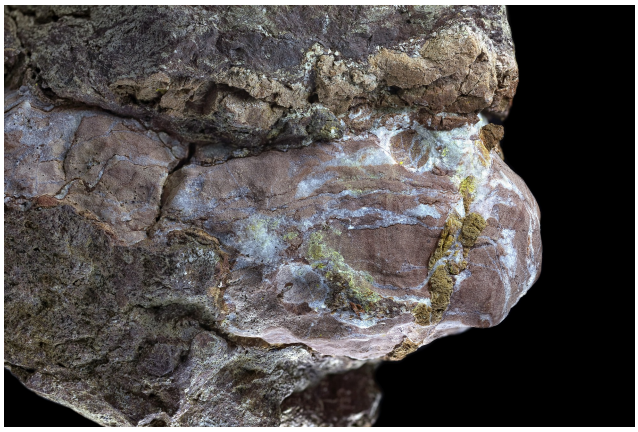

Figure 19: Sample 3. Sample a

Red limestone with white streaks.

The sampling point for sample a) can be seen in the right part of the image.

Image width: 8.3 cm

Photo: Matthias Hanke Collection

Sample 3 documents advanced infiltration of the xenolith by magmatic fluids. The white veins consist of >57 wt% amorphous silicate. indicating rapid quenching of highly viscous. H_2O-saturated infiltrates. The analcime–natrolite–thomsonite assemblage again records hybridization between magmatic alkalis and carbonate-derived Ca.

The occurrence of celadonite represents a key reaction: Fe-oxides in the limestone were reduced under hydrothermal conditions and incorporated, together with magmatic K, into sheet silicate structures. This marks the transition from purely thermal marbling to chemical replacement (metasomatism).

Endometamorphic zone and monomineralic analcime

Figure 20: Sample 3. Sample b
Red layer with a coarse structure.
The sampling point for sample b) is visible in the center.

Image width (cm): 4.1

Photo: Matthias Hanke Collection

On the magmatic side of sample 3, a red, coarse-grained layer occurs at the limestone contact. Phase analysis shows dominantly analcime, with minor calcite likely representing preparation-related contamination. This layer also contains an amorphous component and represents the endometamorphic zone. The dominance of analcime indicates the persistence of magmatic alkaline chemistry up to the immediate contact, while red pigmentation and coarse texture reflect intense hydrothermal interaction and Fe migration from the limestone, which promoted analcime phenocryst growth.

Subsample (c) consists exclusively of analcime and shows a significant amorphous fraction.

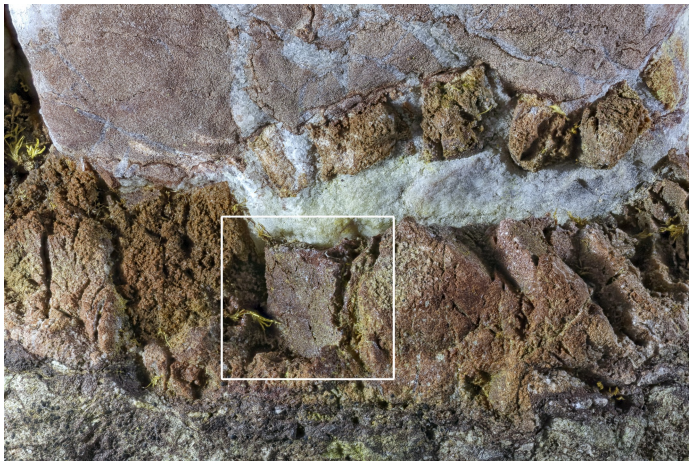

Figure 21: Sample 3. Sample c
Platy-formed analcime region just below a small white marbel layer.

Image width (cm): 3.3
Photo: Matthias Hanke Collection

The discovery of monomineralic, platy analcime at the immediate contact—separated from the xenolith by a small marbled limestone layer—is highly significant. Above this marbled layer, chimney-like structures occur, similar to those in sample 1. The platy analcime marks the peak of hydrothermal activity triggered by fluids released from the rapidly cooling magma. The persistence of amorphous material throughout the contact zones indicates rapid quenching, which preserved high-pressure magmatic phases such as analcime.

The platy morphology of the analcime is not interpreted as a pseudomorph after plagioclase, as the crystal dimensions significantly exceed those of primary plagioclase laths in the host magma. Instead, this texture records directed crystal growth from a highly H_2O-saturated residual melt–fluid phase within the contact zone. The combination of monomineralic analcime growth and high amorphous fractions demonstrates the existence of a mobile, analcime-normative melt–fluid phase during limestone interaction.

Synthesis
Samples 1–3 document a continuous increase in interaction intensity: from purely thermal buffering (isochemical marbling, sample 1), through incipient hybridization (sample 2), to metasomatic infiltration of the xenolith (sample 3). The persistence of analcime across all zones demonstrates the dominance of an H_2O-saturated alkaline magmatic chemistry that remains stable even under extreme carbonate-contact conditions.

Analytical methods
Microscopic investigations were performed using reflected-light stereomicroscopes.

X-ray diffraction (XRD) analyses were conducted using a Panalytical PW 3710 diffractometer with a Cu anode operated at 40 kV and 40 mA. Data acquisition and crystallographic phase analysis were performed using the ADM-Suite V10 software. Phase identification was based on the ICDD PDF-5 database.

Scanning electron microscopy (SEM) and energy-dispersive X-ray spectroscopy (EDX) investigations were performed with a JEOL IT500 instrument. Polished sections were used for

analysis. To avoid interference with the chemical signature, the samples were analyzed uncoated at an acceleration voltage of 10 kV.

Geological Discussion and Conclusions

The phase-analytical investigations document a multistage magmatic evolution transitioning into pervasive autometasomatic (deuteric) alteration. The entire sequence developed under closed-system conditions, requiring no external material input (e.g., seawater or groundwater). In such a system, the volatiles required for secondary mineral formation are derived internally from the magma. Since water and carbon dioxide are not incorporated into early anhydrous phases (olivine, pyroxene), they become progressively enriched in the residual melt until saturation is reached during cooling. The released magmatic fluids remain trapped within the rock framework, reacting directly with the primary minerals through autohydration and carbonation.

This evolution is subdivided into the following stages:

Main Magmatic Stage (> 800 °C): Formation of the primary mineral framework, dominated by clinopyroxene and anorthite-rich plagioclase.

Late-Magmatic Stage (< 660 °C): Crystallization of primary analcime from the water-saturated residual melt. During this stage analcime, plagioclase and clinopyroxene coexist in thermodynamic equilibrium.

Early Hydrothermal Stage (ca. 400 °C–200 °C): Progressive autometasomatism follows one of two distinct pathways depending on the CO_2 fugacity of the fluid phase:

Zeolitic Pathway ($X_{CO_2} < 0.02$): If the magmatic fluid is predominantly aqueous, the reaction of H_2O with the primary assemblage leads to the formation of thomsonite and natrolite.

Carbonate Pathway ($X_{CO_2} > 0.02$): If the fluids are enriched in CO_2 — potentially due to the interaction between the magma and red Jurassic limestone— carbonation occurs. In this closed system, the primary assemblage reacts to form a stable paragenesis of calcite, natrolite and montmorillonite.

Late Hydrothermal Stage (ca. 150 °C–50 °C): Very low-grade zeolite formation (zeolite facies) continues within the closed system as temperatures decline.

Parallel to these internal processes, hydrothermal activity may occur in externally open systems (e.g. fractures and veins). also producing zeolite-facies assemblages. In these environments natrolite and thomsonite dominate, whereas laumontite and heulandite are restricted to more SiO_2-rich domains.

Tectonic and Petrogenetic Implications
The coexistence of primary analcime and Upper Jurassic red limestone xenoliths serves as a precise barometer of regional tectonic conditions. The thermodynamic stability of analcime at 5–6 kbar, combined with the purely physical recrystallization of calcite (marbling), requires that magma–xenolith interaction occurred at crustal depths of approximately 15–20 km. This implies a geodynamic process that transferred Upper Jurassic sediments to mid-crustal levels prior to the

intrusion of water-saturated alkaline magmas. The preservation of this high-pressure paragenesis, together with high amorphous contents (glass phases) in the contact zones, indicates subsequent rapid ascent, which kinetically inhibited subsolidus reactions and preserved metastable phases.

The results presented here contradict earlier interpretations of the Rothplattenbach magmatites as pillow lavas formed in shallow marine environments. Typically, pillows form at the Earth's surface through contact with free water. However, for primary analcime to be preserved, the magma must not have left the high lithostatic pressure environment of the middle crust. The presence of primary analcime in a basaltic magmatite is a definitive indicator of crystallization under high pressure, as analcime is only stable as a primary phase from a melt at pressures exceeding 5 kbar (~15–20 km depth) and in the presence of water. If such a rock nevertheless exhibits pillow morphologies, this can be explained by intrusions into wet sediment ("intrusive pillows").

In this scenario, the magma is emplaced at a depth where the overburden pressure remains sufficiently high (> 5 kbar). There, it encounters water-rich, unlithified sediments. Despite the depth, the pore water within the sediment creates an extreme temperature gradient. The magma reacts physically as it would at the surface: it forms a rapidly cooling, glassy skin (quench margins) that inflates into pillow-like structures due to subsequent magmatic pressure. Since the rock solidifies at this depth, analcime can crystallize directly from the hydrous basaltic melt and remain stable.

In a "normal" stratified crust at 15–20 km depth (middle crust), sediments would long since have been metamorphosed into gneisses or schists. However, in a subduction zone, water-rich seafloor sediments are actively dragged to great depths. Large volumes of water-saturated sediments can be transported along the subduction interface (subduction channel) to depths of 20 km or more before they are fully dehydrated or metamorphosed. These zones are often characterized by extremely high pore fluid pressure, which delays the lithification of the sediments. Consequently, the rising magma encounters a tectonic mélange of "fresh," water-rich material within the middle crust.

The Arosa Zone is classically interpreted as such a tectonic mélange. Our model suggests that the alkali-basaltic magma intruded into this accretionary wedge (or a similar tectonic stack) while it was still in an active phase of deformation and burial. There, the melt encountered hydrous units that had been tectonically transported to depths corresponding to 5–7 kbar. In this environment, the magma would form typical "intrusive pillows" or peperites as the water undergoes abrupt expansion.

The investigated xenoliths consist of pure limestone and show no glass content (no melting/anatexis) and no significant silicification or skarn mineralization. The presence of primary analcime limits the magma temperature during crystallization to below approx. 650 °C. This relatively "cool" temperature of the water-saturated basaltic melt explains why the limestone xenoliths were not marbleized (in the sense of high-T skarns) and did not react with the basalt to form Ca-silicates (such as wollastonite or garnet). The limestone remained chemically largely inert. If these limestones existed as unlithified or water-saturated masses at the time of intrusion at 15–20 km depth, the pillow morphology resulted from the mechanical interaction with the "soft" limestone host under high lithostatic pressure. Here, the pillow shape is not the result of "flow in water" but

rather of "expansion into a ductile medium." Jordan et al. (2008) and Drewes et al. (1961) describe similar phenomena where magma intrudes into water-saturated sediments, where plastic deformation of the sediment facilitates the pillow shape. Models of subduction channels (e.g., Gerya et al., 2002; Guillot et al., 2009) demonstrate that sediments can be transported as "lubricants" to these exact depths before they fully dehydrate.

Interaction with Carbonate Xenoliths

A key aspect of this study is the interaction between the magma and carbonate xenoliths. Our data indicate the following:

1. Pressure-Suppressed Decarbonation: During the initial magmatic stage, high ambient pressure (> 5 kbar) suppressed decarbonation reactions, thereby preventing the formation of classical skarn minerals such as wollastonite.
2. Infiltration Metasomatism and Carbonation: As hydration progressed, infiltration metasomatism occurred. Magmatic, analcime-normative fluids penetrated the xenoliths, forming celadonite (via the reduction of iron oxides within the red limestone) and hybrid zeolites (thomsonite). Simultaneously, the introduction of CO_2 from the limestone into the adjacent magmatic system triggered local carbonation of the primary assemblage, resulting in the characteristic calcite–natrolite–montmorillonite reaction zones.
3. Metasomatic Displacement: The magma did not assimilate the limestone on a large scale but displaced it metasomatically. This confirms that the alkaline character of the magma is a primary feature of the mantle source rather than a result of crustal contamination.

Regional Context

Comparison with the Hegau, Kaiserstuhl, Blairmorites, Col de la Madone, and the Monzoni complex indicates that the crystallization of primary analcime follows strict physicochemical laws. Magmas of the European Cenozoic Rift System (ECRIS) appear to generally ascend water-saturated from metasomatically modified mantle domains.

The Rothplattenbach magmatite provides a compelling example of the transitional zone between mid-crustal crystallization and hydrothermal self-alteration. It uniquely demonstrates how a closed magmatic system can bifurcate into either zeolitic or carbonate-dominated alteration pathways, depending on the localized availability of CO_2 derived from xenolith interaction.

Acknowledgements
The authors thank RMS Kempten for providing access to their XRD laboratory and for supporting the phase-analytical investigations. We are particularly grateful to Mr. Johannes Weber for his significant time and expertise in performing the SEM/EDX analyses using the JEOL IT500.

This research is part of a broader study on the mineralogy and geology of the Allgäu region, initiated by the association D'Allgaier Stoiklopfer e.V. The authors also wish to thank the anonymous reviewers for their critical and constructive evaluation of the manuscript.

References

Baier J (2020) Das Urach-Kirchheimer Vulkangebiet der Schwäbischen Alb. Aufschluss 71(4):224–233

Drewes HF. Fraser GD. Snyder GL. Barnett HF Jr (1961) Geology of Unalaska Island and adjacent insular shelf. Aleutian Islands. Alaska. US Geol Surv Bull 1028-S:583–676

Gerya T (2022) Numerical modeling of subduction: State of the art and future directions. Geosphere 18(2):500–553

Gerya TV. Stöckhert B. Perchuk LL (2002) Exhumation of high-pressure metamorphic rocks in a subduction channel: A numerical simulation. Tectonics 21(6):1056. doi:10.1029/2002TC001406

Geyer M. Gwinner M (2011) Geologie von Baden-Württemberg. 5th edn. Schweizerbart. Stuttgart

Gottardi G. Galli E (1985) The Zeolites. Minerals and Rocks. vol 18. Springer. Berlin Heidelberg New York

Greenwood HJ (1967) Wollastonite: Stability in mixtures of H2O and CO2 at total pressures up to 50.000 bars. Am Mineral 52:1669–1680

Guillot S. Hattori K. Agard P. Schwartz S. Vidal O (2009) Exhumation Processes in Oceanic and Continental Subduction Contexts: A Review. In: Lallemand S. Funiciello F (eds) Subduction Zone Geodynamics. Springer. Berlin. pp 175–205

Gupta AK. Fyfe WS (1975) Leucite-survival: The alteration to analcime. Chem Geol 15(3):213–221

Huckenholz HG (1977) Geology and Petrology of the Hegau Volcanic Province. Fortschr Mineral 55(1):155–174

Huth T. Junker B (2005) Hegau – Geologische Kostbarkeiten. LGRB-Informationen. Freiburg i. Br.

Jordan BR. Fowler AR. Mahmoud BED. El-Saiy AK. Abdelghanny O (2008) Peperites and associated pillow lavas subjacent to the Oman Ophiolite. J Volcanol Geotherm Res 173:303–312

Karlsson HR. Clayton RN (1991) Analcime phenocrysts in igneous rocks: Primary or secondary? Evidence from oxygen and hydrogen isotopes. Am Mineral 76:189–199

Karlsson HR. Clayton RN (1993) Analcime phenocrysts in igneous rocks: Primary or secondary? — Reply. Am Mineral 78:225–226

Kerrick DM (1974) Review of Metamorphic Mixed-Volatile Equilibria. Am Mineral 59:729–762

Kim KT. Burley BJ (1971) Phase equilibria in the system NaAlSi3O8 – NaAlSiO4 – H2O with special emphasis on the stability of analcite. Can J Earth Sci 8:311–337

Konya P. Szakáll S (2011) Occurrence. composition and paragenesis of the zeolites and associated minerals in the alkaline basalt of a maar-type volcano at Haláp Hill. Balaton Highland. Hungary. Mineral Mag 75:2869. doi:10.1180/minmag.2011.075.6.2869

Kristmannsdóttir H. Tómasson J (1978) Zeolites zones in geothermal areas in Iceland. In: Sand LB. Mumpton FA (eds) Natural Zeolites: Occurrence. Properties. Use. Pergamon. New York. pp 277–284

Kushiro I (1969) The system forsterite-diopside-silica with and without water at high pressures. Am J Sci 267-A:269–294

Liou JG. de Capitani C. Frey M (1991) Zeolite equilibria in the system CaAl2Si2O8 - NaAlSi3O8 - SiO2 – H2O. NZ J Geol Geophys 34:293–301

Luhr JF. Kyser TK (1989a) Primary and secondary phlogopites and clinopyroxenes in alkaline lavas from the Colima Graben and Southern Guadalajara. Mexico. Contrib Mineral Petrol 102:147–160

Luhr JF. Kyser TK (1989b) Primary analcime in intermediate magmas from the Colima Volcanic Complex. Mexico. Contrib Mineral Petrol 102:420–439

Mäder U (1983) Die Geochemie der Tiefengesteins-Xenolithe des Uracher Vulkangebietes. Dissertation. ETH Zürich

Pearce TH (1970) The analcite-bearing volcanic rocks of the Crowsnest Formation. Alberta. Can J Earth Sci 7:46–66

Pearce TH (1993) Analcime phenocrysts in igneous rocks: Primary or secondary? – Discussion. Am Mineral 78:222–224

Peters Tj. Luth WC. Tuttle OF (1966) The stability of analcime and its neighbors. Am Mineral 51:736–753

Reiser KA (1889) Über die Eruptivgesteine des Allgäu. Dissertation. Universität München

Richter D (1974) Grundriß der Geologie der Alpen. De Gruyter. Berlin

Richter D (1984) Allgäuer Alpen. Samml Geol Führer. vol 77. 3rd edn. Borntraeger. Berlin Stuttgart

Roux J. Hamilton DL (1976) Primary analcite from igneous rocks. J Petrol 17(2):244–257

Schiemenz S (1960) Fazies und Paläogeographie der subalpinen Molasse zwischen Bodensee und Isar. Beih Geol Jahrb 38. Hannover

Schleicher H (1994) The Urach-Kirchheim volcanic field. In: Chenet PY (ed) Volcanism in the Upper Rhine Graben and its surroundings. l'Ecole Nationale Supérieure du Pétrole et des Moteurs. Paris

Scholz H (2016) Bau und Werden der Allgäuer Landschaft. Schweizerbart. Stuttgart

Scholz H (ed) (2023) Wetzstein. Erz und Kohle. Nutzbare Gesteine. Minerale und andere Rohstoffe aus den Allgäuer Alpen. Schweizerbart. Stuttgart

Skippen GB (1971) Experimental data for reactions in siliceous marbles. J Geol 79(4):457–481

Spürgin S. Weisenberger TB. Marković M (2019) Zeolite-group minerals in phonolite-hosted deposits of the Kaiserstuhl Volcanic Complex. Germany. Am Mineral 104(5):659–670. doi:10.2138/am-2019-6703

Thompson AB (1971) PCO2 in low-grade metamorphism; zeolite. carbonate. clay mineral. prehnite and pumpellyite facies. Contrib Mineral Petrol 33:145–161

Wassermann A (1982) Stabilitätsbeziehungen von Akermanit (Ca2MgSi2O7) – Gehlenit (Ca2Al2SiO7) Mischkristallen in Gegenwart einer binären H2O – CO2 Gasphase. Dissertation. LMU München

Wilson M. Downes H (1991) Tertiary-Quaternary extension-related alkaline magmatism in Western and Central Europe. J Petrol 32(4):811–849

Wimmenauer W (1962a) Die Phonolithe und Tinguaite des Kaiserstuhls. Mitt Bad Landesver Naturk Naturschutz NF 8:85–91

Wimmenauer W (1962b) Beiträge zur Petrographie des Kaiserstuhls. Teil IV: Die Phonolithe und Tinguaite. Neues Jahrb Mineral Abh 98:367–476

Wimmenauer W (1985) Petrographie der magmatischen und metamorphen Gesteine. Enke. Stuttgart

Wimmenauer W (2003) Der Kaiserstuhl: Geologische Beschreibung eines Vulkangebirges. LGRB. Schweizerbart. Stuttgart

Yoder HS. Tilley CE (1962) Origin of basalt magmas: An experimental study of natural and synthetic rock systems. J Petrol 3(3):342–532